WORLD CONFERENCE ON TIMBER ENGINEERING 2025
BRISBANE, AUSTRALIA
Advancing Timber for the Future Built Environment

PRELIMINARY INVESTIGATION ON THE STRUCTURAL AND HYGROTHERMAL PERFORMANCES OF CLT WITH AIRGAPS

Yutaka Goto[1], Robert Jockwer[2]

ABSTRACT: Cross laminated timber (CLT) has been a major contributor to the expansion of the technical possibilities of timber constructions. While CLT has advantages, the production of CLT requires extensive raw material input compared to the actual needs regarding structural capacity. It is expected that the required load bearing capacity can be achieved by using less raw material if the timber lamellas are arranged properly with gaps in between. Different configurations with different material efficiency result in different structural and hygrothermal performance of the panels. The overall goal of the project described in this paper is to investigate the raw material saving potential for a multi-story structure with CLT panels with airgaps. For this purpose, the shear, bending, and water vapor permeability performances of 3-ply and 5-ply CLT panels with various airgap configurations have been investigated in experiments and in numerical and analytical models. Based on the results, the load bearing structure of an 8-story residential building was designed with CLT panels with airgaps. The structure was designed to satisfy the performance requirements according to Eurocodes and for moisture safety. The result shows that the material saving potential is at maximum 46% for the floor and 29% for the wall. In order to further optimize the CLT panels and verify the results, more experiments on more variety of airgap configurations will be needed.

KEYWORDS: CLT, material efficiency, airgap, shear performance, vapor permeability

1 – INTRODUCTION

The construction industry has been a major contributor to the Green House Gas emissions. Larger timber constructions are gaining more and more attention in many regions for the carbon storage capacity and renewability of timber. Cross laminated timber (CLT) has largely contributed to the expansion of the technical possibilities of timber construction. As the interest in mass timber structures with CLT grows globally, there is a need for awareness on the resource availability and efficiency. Although wood is a renewable resource in principle, it needs to be produced from sustainably maintained forests and it needs to be utilized as efficient as possible in order to meet the increasing demands and to prevent the deterioration of the carbon storage potential of the forests.

2 – BACKGROUND AND OBJECTIVE

2.1 BACKGROUND

We are seeing escalating urbanization and the need for more constructions in densely populated areas both globally and locally [1]. Meanwhile, the construction industry has been a major contributor to the GHG [2]. Timber constructions (including both “pure” and hybrid timber constructions) have been gaining more and more presence in the global construction industry [3, 4].

The major drivers of this significant growth of the timber construction industry especially in regions with a sufficient local resource supply are: (1) there are well-experienced wood-processing and timber construction companies, (2) the cost competitiveness of multi-story timber constructions has come very close to other alternatives such as concrete as the market experience increases [5] and (3) there is the growing consciousness of environmental sustainability and timber is seen as a more favourable option for its carbon neutrality, renewability and circularity.

This great advancement of the timber construction industry is primarily supported by research and developments in structural and fire safety technologies. Among various technologies, cross laminated timber (CLT) has been a major contributor of the expansion of

[1] Yutaka Goto, Dept. of Architecture and Civil Engineering, Chalmers University of Technology, Gothenburg, Sweden, yutaka@chalmers.se

[2] Robert Jockwer, Institute of Steel and Timber Construction, TUD Dresden University of Technology, Dresden, Germany, robert.jockwer@tu-dresden.de

https://doi.org/10.52202/080513-0277

the technical possibilities especially in structural capacity [6].

There are various advantages of CLT. The structural advantages are: (1) it has a high loadbearing capacity, (2) the structural planning is relatively simple and similar to concrete structure. The hygrothermal advantages are: (1) it has a thermally insulating function thanks to its massive structure, (2) it has a large moisture sorption capacity and moderate heat capacity due to the high volume of timber, (3) it has a moderate vapour permeability and it can work as vapour retarder and (4) it has a higher dimensional stability under varying humidity conditions compared to solid wood. The environmental advantages are: (1) it uses timber as a renewable material, (2) it contributes to the increased carbon storage in urban areas and (3) it can utilize lower quality timber lamellas by mixing them with other lamellas within one panel, and thus it contributes to a more efficient use of resources.

While CLT constructions have its advantages, the production of CLT requires large raw material input compared to the typically resulting structural capacity. It can be expected that depending on the loading situations, the required performance can be achieved by using less raw material if the timber lamellas are arranged with gaps in between (see Figure 1). Another practical issue from the production perspective is that often lamellas of relatively high quality are used to fill the necessary volume of panels to keep the logistics of the production simple.

When considering the global trend of timber constructions, it is crucial to improve the efficiency in the resource management. Wood is also an attractive alternative as a renewable energy source. As the energy sector seeks to grow the share of the renewable energy, there could be a resource conflict between the two sectors which may potentially lead to local and/or global shortage of resource [7].

In the present study, CLT with airgaps between lamellas in cross layers is proposed. Figure 1 shows some examples of airgap configurations of such CLT panels. Different airgap configurations result in different structural and hygrothermal performance of the panels. The structural performance is of relevance for all load bearing elements, while the hygrothermal performance is most relevant for exterior walls to ensure the energy performance and moisture safety of the building. It should be considered that the introduction of airgaps may cause a number of complications e.g. in the panel production, joint design, onsite workability, and fire resistance. Therefore, the use of panels with air gaps is only competitive in industrial upscaling if sufficient material saving is achieved.

While there has been some limited research on the mechanical properties of CLT panels with airgaps [8, 9], its rolling shear performance and its sensitivity to the arrangement of airgaps across different layers has not been studied. Furthermore, the hygrothermal properties of solid CLT panels and building envelopes with them have been studied [10, 11], there has been no study on the hygrothermal properties of CLT panels with airgaps.

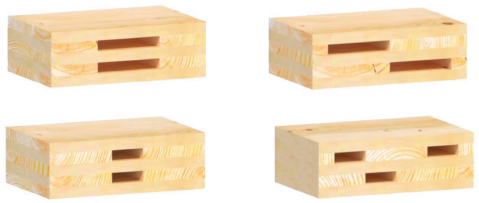

Figure 1. Examples of airgap configurations in CLT panels.

2.2 OBJECTIVE AND LIMITATIONS

The objective of this paper is to summarize the studies on the impact of the airgaps in CLT on the structural and hygrothermal performance and to provide a preliminary investigation on the raw material saving potential for a multi-storey building made of CLT panels with airgaps. This includes the following aspects:

- Shear performance by analytical prediction and its validation by small-scale test and FEM.
- Bending performance by large-scale test.
- Vapor permeability performance by analytical prediction and sensitivity study by dynamic heat and moisture transfer modelling.
- Material saving potential analysis by a structural analysis case study of a whole building by applying the analytical predictions.

This study has the following limitations:

- Each configuration has airgaps only in the cross layers, that are considered to be arranged horizontally in the structure. This is for avoiding vertically continuous air channels (when the panel is used as a wall), which may significantly impact the hygrothermal and fire resistance performance due to the vertical air circulation.
- The work is limited to the wood species spruce.

https://doi.org/10.52202/080513-0277

- The study is based on the Swedish context with regard to hygrothermal requirements and to the framework of Eurocodes.

In the following chapters the Shear, Bending, and Vapor permeability performances are presented and concluded in the material saving potential analysis.

3 – SHEAR PERFORMANCE INVESTIGATION

3.1 SMALL-SCALE SHEAR TEST

Rolling shear tests for CLT are specified EN 16352 [12]. In order to evaluate the impact of airgaps in CLT panels similar tests have been carried out with slight modifications of geometry and configuration but following the general principles of the inclined shear test according to EN 16352 and EN 408 [13]. Six different configurations (one solid panel without airgaps and five panel types with different airgap configurations) were produced in the workshop of Chalmers University of Technology. Figure 2 shows the configurations.

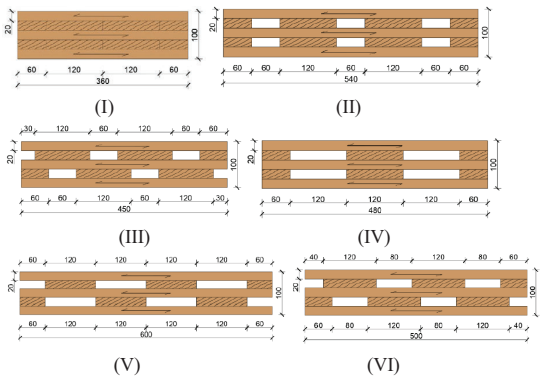

Figure 2. Configurations of specimens for the rolling shear test

PVAC-based adhesive was applied between the wood lamellas (conditioned to a moisture content of approximately 12%), and they were pressed tightly together by using hand-screw steel clamps. The wood species for the specimens was spruce and boards had a strength class of C24 [14]. In each specimen, the two opposite diagonal edges were sawn at an angle in order to be placed at the intended inclination in the universal testing machine with a maximum capacity of 250 kN, see Figure 3.

The inclination angle α varied depending on the configuration, thickness, and length of the specimens since the vertical loading axis was properly aligned to the center of the specimen according to Equation (1).

$$\alpha = arctan\left(\frac{h-10}{L}\right) \quad (1)$$

where h (mm) is specimen thickness, and L (mm) is specimen length. The 10 mm in Equation (1) is used to adjust for the support conditions and load introduction via special steel stamps. A black speckle pattern on white background was applied for the ARAMIS optical system [15] to monitor the surface deformation and compute strains. The loading rate was set at 0.5 mm/min. For each configuration 4-5 specimens were tested.

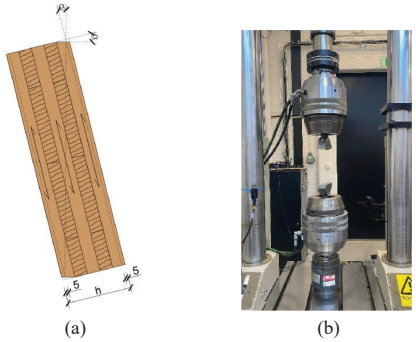

Figure 3. Test configuration of the rolling shear test: Set up of the inclined specimen (a), universal testing machine for the rolling shear test (b).

By modifying the formula in from EN 16352 [12], the effective rolling shear strength of the specimens with airgaps can be calculated based on Equation (2).

$$f_{r,eff} = \frac{F_{max} \cdot \cos\alpha}{l_c \cdot b} \quad (2)$$

where $f_{r,eff}$ is the effective rolling shear strength (N/mm^2), F_{max} (N) is the maximum load obtained in testing, b (mm) is the width of the test specimen, l_c (mm) is the effective rolling shear length of test specimens (length of the cross-layer bond lines), α is the inclination of the specimen (see Equation (1)).

Furthermore, the smeared shear modulus of the specimen (including parallel and rolling shear effects) can be calculated according to Equation (3) in order to account for the reduction of the bond line length and cross-layers.

$$G_{r,eff} = \frac{(F_2 - F_1) \cdot \cos\alpha \cdot h}{(u_2 - u_1) \cdot l_c \cdot b} \quad (3)$$

where $G_{r,eff}$ is effective rolling shear modulus (N/mm^2), F_2 - F_1 (N) is load increment between $0.3 \cdot F_{max}$ and $0.6 \cdot F_{max}$, u_2 - u_1 (mm) is the deformation increment according to F_2 - F_1, h (mm) is the thickness of the specimen.

https://doi.org/10.52202/080513-0277

3.2 NUMERIAL ANALYSIS

Models of the shear test were created and analyzed for all tested configurations with the Finite Element Method (FEM) in ABAQUS/standard [16]. All the layers were constructed as 3D deformable elements with a solid shape and extrusion type. The material was modelled as orthotropic with engineering constants corresponding to C24 properties. Based on measurements of individual boards of the specimens, the average density was set to 490 kg/m^3. The bondline was not explicitly modelled, instead the interactions between neighboring layers were modeled as tie constraints. No interaction was modeled between cross-layers since the cross-layers in specimens were not edge-bonded. Figure 4 shows the mesh of Configuration II as an example of a model of a specimen.

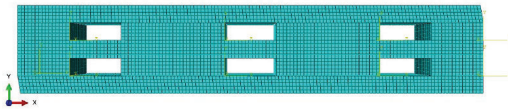

Figure 4. Mesh division for Configuration II

3.3 RESULT AND DISCUSSION

As an example of the test results, Figure 5 (a) and (b) show the load-deformation curves (4 specimens) and strain distribution (1 specimen) for Configuration III, respectively. The failure mode of most of the tests was shear failure in the cross layer and the bondline. Figure 5 (c) shows the failure pattern of the Configuration III specimen from Figure 5 (b). The overall summary of effective rolling shear strength (based on the full specimen length), net rolling shear strength (based on the net length of the cross-layers), effective rolling shear modulus, and net rolling shear modulus is presented in Table 1.

Generally, there is a correlation between the net shear modulus and the net shear strength. Configuration III, which has 60 mm shifted airgaps with a 20 mm overlap of lamellas across the cross layers (see also Figure 5 (c)), showed the highest net rolling shear modulus. In terms of effective shear strength along the entire specimen of CLT with airgaps, Configuration III showed the highest effective shear strength, which is 29% lower than Configuration I with a solid panel. 13% of material can be saved in Configuration III compared to Configuration I, hence there is an over proportional reduction of the structural performance. Configurations II and III have the same material saving of 13% compared to a solid panel. However, Configuration III has overlaps of lamellas across cross layers and showed a 23% higher net and effective shear strength Configuration II. Configurations with overlapping lamellas across cross layers (Configurations III and VI) generally showed a higher rolling shear modulus and shear strength than configurations without overlapping cross layers (II, IV, and V).

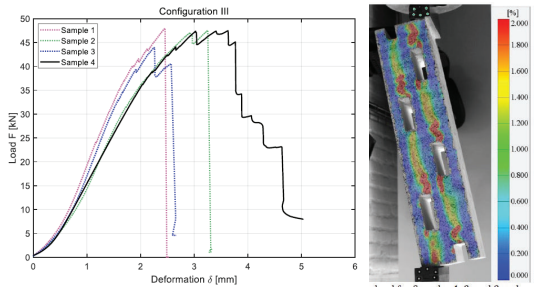

(a) (b)

(c)

Figure 5. Test results of Configuration III: Load deformation curves (a), strain distribution on the specimen surface right before failure (b), crack pattern of the specimen (c).

Table 1: Shear strength and shear modulus results of the 6 configurations of CLT with and without airgaps

Config.	*Effective rolling shear strength (MPa)*		*Net rolling shear strength (MPa)*		*Effective shear modulus (MPa)*		*Net shear modulus (MPa)*	
	$f_{r,eff,mean}$	*(COV)*	$f_{r,net,mean}$	*(COV)*	$G_{eff,mean}$	*(COV)*	$G_{net,mean}$	*(COV)*
I	1.31	14%	1.31	14%	72.1	7%	72.1	7%
II	0.75	12%	1.13	12%	42.5	5%	63.8	5%
III	0.93	4%	1.39	4%	50.4	14%	75.6	14%
IV	0.66	9%	1.32	8%	35.0	8%	69.9	8%
V	0.57	23%	1.14	23%	32.1	20%	64.3	20%
VI	0.80	11%	1.33	11%	44.1	10%	73.4	10%

In the FEM models the impact of the airgap configurations on the stress distribution in the specimens could be analyzed. As observed in the experimental data, the introduction of airgaps induces stress concentrations that are proportional to the material saving. Further, from the FEM result the difference in the stress distribution between Configurations II and III (same material saving and aligned/overlapping lamella position across cross layers) can be analyzed.

https://doi.org/10.52202/080513-0277

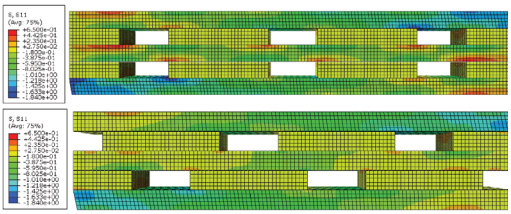

Figure 6. The stress contour of the parallel to grain stresses (S11) for Configurations II (top) and III (bottom)

The stress contour of the parallel to grain stresses (S11) for Configurations II and III are shown in Figure 6. As can be seen, the magnitude of the normal stress S11 in Configuration II is significantly larger than Configuration III. In Configuration II a higher stress concentration is observed in the corner of the air gaps. Meanwhile, in Configuration III the stress distribution is smoother. The stress perpendicular to the grain S22 and the shear stress S23 showed more similar values for both configurations.

4 – BENDING PERFORMANCE INVESTIGATION

4.1 LARGE-SCALE BENDING TEST

Bending tests with loads perpendicular to the plane according to EN 16351 [12] were carried out (see Figure 7). Three different configurations (A, B, and C, see Figure 8) were produced at an industrial manufacturing environment with 3 specimens for each configuration. All configurations were made of lamellas of 120 mm width and 20 mm thickness and consisted of 5 layers. Configuration A is a solid panel with no airgap (2000 mm long, 200 mm wide, and 100 mm thick). Configurations B and C have 60 mm wide and 120 mm wide, symmetric airgaps in the cross layers, respectively.

The CLT was produced with Polyurethane adhesive, the wood species was spruce and the lamellas were of strength class C24. The tests were performed as 4 point bending tests in the flexible rig of the Structural Testing Laboratory of Chalmers University of Technology. In addition to local LVDT measurements, also the ARAMIS optical system was used to monitor the surface deformation on the front surface (see Figure 7). The test was carried out with a reloading cycle. In the first load cycle the load was increased to 8-11 kN depending on the configurations, then the specimens were unloaded to 1-2 kN, and finally loaded until failure. The tests were carried out deformation controlled with a loading rate of 5 mm/min.

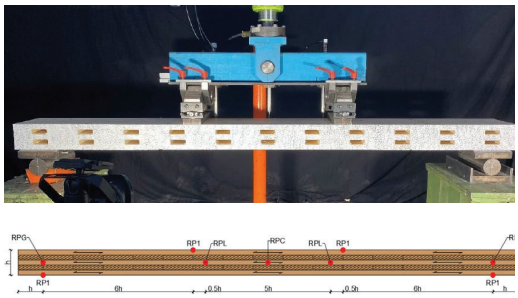

Figure 7. Test setup for large-scale bending tests of a configuration (B) specimen and location of measurement points.

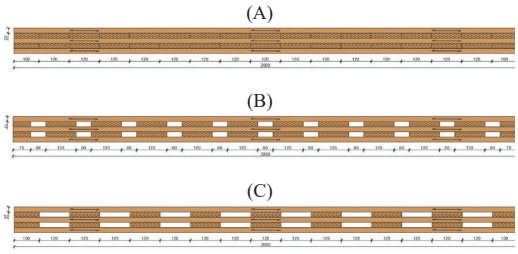

Figure 8. Three configurations of CLT without and with airgaps.

4.2 RESULT AND DISCUSSION

The bending strength, the bending stiffness, and the smeared, effective global MOE of the full-scale bending tests are summarized in Table 2. The bending strength was derived using the effective analytical bending stiffness of the three configurations based on the γ-method and an MOE of $E_m = 11'000$ (N/mm^2) with $EI_{eff,A} = 12{,}45 \cdot 10^{10}$ (Nmm^2) (A), $EI_{eff,B} = 11{,}63 \cdot 10^{10}$ (Nmm^2) (B), and $EI_{eff,C} = 11{,}02 \cdot 10^{10}$ (Nmm^2) (C).

Table 2: Bending strength and stiffness of the 3 configurations of CLT with and without airgaps

Config.	*Effective bending strength (MPa)*		*Effective experimental bending stiffness (·10^{10}Nmm^2)*		*Effective experimental local MOE (kN/mm^2)*	
	$f_{m,eff,mean}$	*(COV)*	$EI_{eff,local,mean}$	*(COV)*	$E_{eff,local,mean}$	*(COV)*
A	43	18%	14.3	7%	10.1	5%
B	50	7%	12.5	5%	9.6	13%
C	39	5%	9.7	14%	7.3	3%

The bending strength is also shown in Figure 9 for the 3 configurations. Several interesting aspects can be seen. First of all, it should be mentioned that bending failure often occurred at local wood characteristics in the tension zone. This is also an explanation for the low bending strength of the first test A1 where failure occurred due to a local knot cluster in the tension zone below one of the load introduction points. Furthermore, the higher bending

https://doi.org/10.52202/080513-0277

strength of the configuration 2 is remarkable. Specimens B1 and B2 failed due to (rolling) shear failure in the support regions. Only specimen B3 failure due to bending failure in the tension zone. Hence, the higher apparent bending strength can be related to the absence of defects in the tension zone and a shift of failure modes.

In the four-point bending test, configuration B with 6 cm airgap between cross layer laminations has a 13% material volume reduction compared to the solid panel of configuration A, and configuration C with 12 cm airgaps has a 19% material volume reduction. In Figure 10 the respective reduction in effective, local bending stiffness $EI_{eff,local}$ is shown for the three configurations. Despite the relatively large scatter in results, it can be observed that the reduction in bending stiffness is approximately linear and lays in between the ratio of the material volume reduction and the reduction in cross-layer bondline length (33% reduction for configuration B and 50% reduction for configuration C).

A simple and conservative approach can be to base the effective bending stiffness on the reduction in cross-layer bondline length as shown in Equation (4).

$$\lambda = \frac{l_{bond}}{l_{bond}+l_{air}} \tag{4}$$

where l_{bond} is the bondline length in the cross layer and l_{air} is the length of the respective airgap.

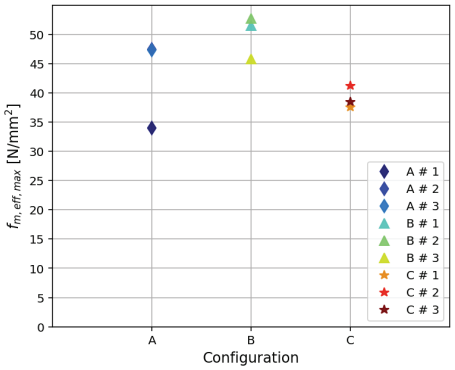

Figure 9. Bending strength of the three configurations in the 4-point bending tests.

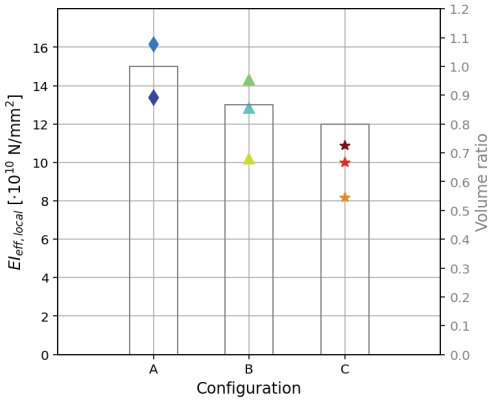

Figure 10. Effective local bending stiffness of the three configurations in the 4-point bending tests (data plots with the left axis) in relation to the respective material volume reduction (bar chart with the right axis).

5 – PERMEABILITY INVESTIGATION

In the hygrothermal investigation, it was aimed at proposing a simple but versatile analytical model to predict the water vapor diffusion resistance factor (μ-value) of a CLT panel with air gaps. Furthermore, transient heat and moisture transfer analysis was performed to evaluate the moisture safety of a building envelope system with such a panel by transient hygrothermal calculations under the Swedish climate.

5.1 METHODOLOGY

Analytical calculation of vapor permeability

The present study introduces the equivalent vapor permeability δ_{eq} (m^2/s) to represent the overall vapor permeability of a panel configuration with a single value at a given relative humidity condition. The analytical model for the calculation δ_{eq} in the panel thickness direction is proposed as an analogical model to the heat bridge model. Figure 11 shows the model of "moisture bridge" model with an example of a panel configuration.

In the model, the cross section of the panel is segmented into sections according to the existence of the airgap in the thickness direction. The vapor resistance of segment n, Z_n (s/m), is calculated as a serial vapor resistance of the wood and air layers in the segment. For example, in the case of the configuration in Figure 11, the vapor resistance of Segment 2, Z_2, is given by Equation (5).

$$Z_2 = \frac{t_a}{\delta_{wood}} + \frac{t_b}{\delta_{air}} + \frac{t_c+t_d+t_e}{\delta_{wood}} \tag{5}$$

https://doi.org/10.52202/080513-0277

where δ_{wood} (m^2/s) and δ_{air} (m^2/s) is the vapor permeability for the respective material. It should be noted that the surface resistance of the vapor diffusion between air and wood (typically 360 s/m for an enclosed "indoor" environment with less air flow at a room temperature) is neglected as it is significantly smaller than the resistance in material layers. Furthermore, diffusion resistance of the glue line is disregarded with the assumption that the glue line is as vapor-open as the solid wood part [17].

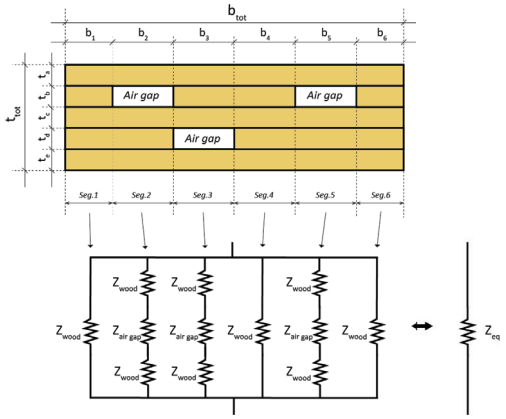

Figure 11. Scheme of the analytical model of the vapor resistance

Then the equivalent diffusion resistance Z_{eq} (s/m) of the entire panel is obtained as a parallel resistance by Equation (6).

$$\frac{1}{Z_{eq}} = \frac{1}{Z_1} \cdot \frac{b_1}{b_{tot}} + \frac{1}{Z_2} \cdot \frac{b_2}{b_{tot}} + \cdots + \frac{1}{Z_n} \cdot \frac{b_n}{b_{tot}} \quad (6)$$

where b_n (m) is the width of segment n, and b_{tot} (m) is the total width of the panel.

Finally, the equivalent vapor permeability, δ_{eq} (m^2/s), is obtained by Equation (7).

$$\delta_{eq} = \frac{t_{tot}}{Z_{eq}} \quad (7)$$

where t_{tot} (m) is total thickness of the panel.

An actual δ_{eq} is obtained when the model it applied to an actual panel configuration. Figure 12 shows the variation of airgap configurations of the CLT panels for the testing the δ_{eq} calculation. Panels (A)-(B) consist of 3 layers of 30 mm thick wooden lamellas. Panels (C)-(F) consist of 5 layers of 20 mm thick lamellas. Each configuration is supposed to have the repetitive airgap pattern when the panel is elongated in the length direction. When assuming a regular climatic condition (around 20ºC and 50%RH) across the entire panel, δ_{wood} and δ_{air} can be given at $5.0 \cdot 10^{-8}$ m^2/s and $2.5 \cdot 10^{-6}$ m^2/s. As a result, Z_{eq}, δ_{eq}, vapor diffusion resistance factor (μ-value), and reduction of μ-value compared to a solid wood of each configuration are obtained as can be seen in Table 3. It should be noted that δ_{wood} is highly dependent on the relative humidity of ambient air, and thus the input value for the calculation may need to consider this when there is a large variation of relative humidity across the panel.

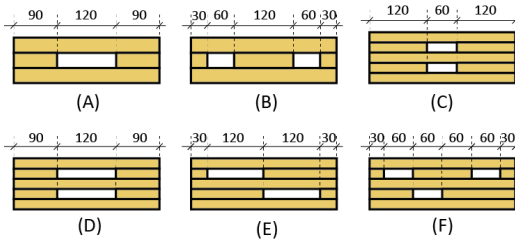

Figure 12. The variation and section geometry (in mm) of airgap configurations of CLT panels for vapor permeability assessment.

Table 3: Vapor resistance, permeability and μ-value of the 6 airgaps configurations

	A	*B*	*C*	*D*	*E*	*F*
Z_{eq} ($\cdot 10^{6}$s/m)	*1.51*	*1.51*	*1.77*	*1.59*	*1.67*	*1.74*
δ_{eq} ($\cdot 10^{-8}m^2/s$)	*5.97*	*5.97*	*5.64*	*6.29*	*5.98*	*5.73*
μ	*42*	*42*	*44*	*40*	*42*	*44*
Decrease of μ	*16%*	*16%*	*11%*	*21%*	*16%*	13%

Moisture safety evaluation by transient heat and moisture transfer simulations

In order to test the impact of the airgap, a dynamic heat and moisture transfer simulation was carried out by WUFI® Pro ver.5.3 [17]. The model was set as a building envelope system with a load bearing timber panel (100 mm) and mineral wool insulation (60 mm) to satisfy the minimum requirement for the U-value under the Swedish building regulation.

As a reference case, a solid CLT panel data by Stora Enso (available in the built-in material database of WUFI) was applied. For a test case, the hygrothermal properties of the Stora Enso CLT panel were modified in the following way: The μ-value (moisture-dependent) was decreased by 15% (the average decrease among configuration C, D, E, and F, see Table 3). The density and moisture sorption capacity were reduced by 13% (average volume ratio of airgap of the 4 configurations). Thermal conductivity of the modified panel was also altered by applying the heat bridge model according to the geometry of the configurations. In this procedure, the thermal conductivity of the airgap in this heat bridge model was calculated based on EN 6946 [19]. As a result, the

https://doi.org/10.52202/080513-0277

thermal conductivity was given at 0.12 W/(m·K). The climatic condition was set with the Gothenburg dataset for 3 years. The impact by the raindrops was disregarded by assuming the application of a façade cladding with a ventilated airgap. Figure 13 shows the one-dimensional mesh division and monitoring position of the simulation model.

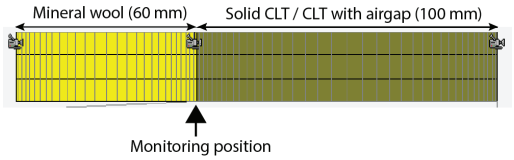

Figure 13. Model geometry and mesh division of the dynamic heat and moisture transfer simulation

5.2 RESULT AND DISCUSSION

Figure 14 (a) shows calculated relative humidity at the interface of the mineral wood and the timber panel for the whole simulation period of three years. Figure 14 (b) shows the result for the period of 800 hours when the position shows the highest relative humidity level. As can be seen in these figures, there is little difference between the cases with and without airgap. This demonstrates that the decrease of μ-value by 15% does not have a major impact when the panel is applied as a part of a building envelope system. Furthermore, the maximum relative humidity at the monitoring position, which is the most sensitive point inside the envelope in terms of moisture accumulation, does not exceed 75%RH and there is no yearly increase in the humidity over the 3-year simulation period. Therefore, no moisture-induced risks (mould growth and wood decay) are expected to occur. Thus, it is concluded that the introduction of a moderate volume of airgaps does not cause hygrothermal risks under the given climatic conditions and envelope design.

For the validation of the analytical model, it is desirable to carry out laboratory tests of vapor permeability measurements with various configurations. The dynamic simulation can be expanded by applying more variety of climatic conditions and envelope design. It should be also considered that cracks in the outer layers could significantly impact the hygrothermal performances if it results in connecting airgaps and ambient air.

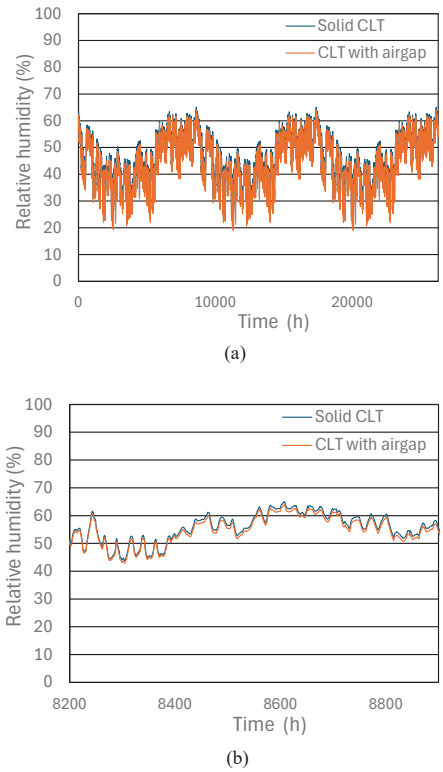

Figure 14. Simulation result of relative humidity of the interface between mineral wood insulation and timber panel: The result of the simulation period of three years (a), the close-up of the result of the period with the highest relative humidity level (b).

6 – MATERIAL SAVINF POTENTIAL INVESTIGATION

Based on these studies on the shear, bending and hygrothermal performance, a material saving potential was investigated to determine where and when it is suitable and most efficient to apply CLT panels with airgaps in a building. The models for the structural and hygrothermal performances obtained from the above investigations were applied in the design for an 8-storey residential case study building. This case study building is based on the worked example by Wood Solutions [20] with some adjustments, such as a simplification of the façade and a more regular floor plan. An illustration of the case study building is shown in Figure 15. The load bearing structure had to be designed to satisfy the performance requirements in the Eurocodes and the moisture safety (the relative humidity inside the building envelope is kept below 75%). For this, a catalogue of 36 panel layups was created with 3-ply and 5 ply panels (thicknesses of 60-200 mm) with different airgap

https://doi.org/10.52202/080513-0277

configurations. This catalogue follows similar existing catalogues from commercial CLT producers.

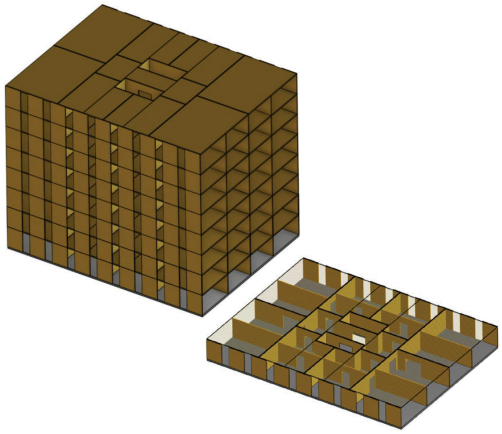

Figure 15. Elevation and layout of the case study CLT building.

The investigation was done with regard to the following criteria: The thickness of the CLT panels is minimized; the airgap is introduced to achieve the highest volume reduction while maintaining the structural requirements; for the panels in the building envelope, an extra transient heat and moisture transfer analysis is carried out with the additional insulation layer under the Swedish climatic conditions.

Using the catalogue and the optimisation criteria, a major material saving potential was observed. The material saving of floor panels (5 variations) ranged between 25% and 46%. It was characteristic to observe that the span of the floor panels differed and a large variation in utilisation ratio. When aiming for an overall constant floor slab thickness in each storey, some panels had a considerably low utilization ratio. For wall panels (11 variations), the material saving ranged between 5% and 29%.

However, this large material saving potential will most likely not be achieved in practice due to the detailing of the floor and wall for connections, detailing for concentrated loads in the elements and so on. In addition, the dynamic performance of the CLT panels with airgaps has to be further analysed.

7 – CONCLUSION AND RECOMMENDATIONS

From the structural investigations, it was found that the presence of air gaps significantly impacts the structural properties of the panels. In four-point bending tests, it was observed that panels with wider air gaps showed increased deflection and decreased stiffness compared to solid panels without air gaps. The result suggests that the stiffness of CLT panels with airgaps can be approximated based on the reduction in cross-layer bondline length. For limit the reduction in effective rolling shear strength it is beneficial to use a shifted airgap configuration between the cross-layers.

When the equivalent vapor permeability from the analytical model is applied in the building envelope model by the transient heat and moisture transfer method with the Swedish climate, it was shown that the sensitivity of the change of the μ-value due to the airgaps is not high for the judgement of the moisture safety of building envelopes.

From the material saving potential investigation, it was shown that air gaps can be applied to a meaningful extent and still satisfy global structural and hygrothermal requirements. However, the local detailing has to be developed and the effect of concentrated loads and the dynamic behaviour has to be further studied.

In order to further optimize the application and verify the results, more experiments on more variety of airgap configurations will be needed as the configuration variation for the structural performance tests was limited. Furthermore, the analytical vapor permeability model needs to be validated with experimental data.

8 – ACKNOWLEDGEMENT

The authors gratefully acknowledge the contributions by Rebecka Nilsson, Tove Nilsson, Anna Moberg, Linda Xiao, Hanna Kurzawinska, Mohammad Tahmasebi, Mohannad Elhajj, Elliot Sterneling, and Tim Schüler through their thesis works and project assistance. Wilhelm Polster and other colleagues at Stora Enso are acknowledged for the continuous discussion for the project development and the support in the specimen production. FORMAS is acknowledged for the grant (grant registration number: 2020-01784) for the execution of the research project.

9 – REFERENCES

[1] S. Angel. “Urban expansion: theory, evidence and practice.” In: Buildings & Cities 4. 1 (2023), pp. 124–138.

[2] UN Environment Program. Golobal Status Report. 2018.

[3] H. Svatoš-Ražnjević, L. Orozco, and A. Menges. “Advanced Timber Construction Industry: A Review of 350 Multi-Storey Timber Projects from 2000–2021.” In: buildings 12. 4 (2022), 404.

[4] S. Pastori, E.S. Mazzucchelli, and M. Wallhagen.

“Hybrid timber-based structures: A state of the art review.” In: Construction and Building Materials 359 (2022), 129505.

[5] J. Swartz Andersen, Y. Goto, M. Englund, H. Johansen, K. Armann Hansen, A. Hollberg, and D. Grotenfelt. “Economic comparison of mass timber and concrete construction in the Nordic region.” In: 13th World Conference on Timber Engineering, WCTE 2023 Vol. 7, pp. 4360-4369.

[6] R. Brandner, G. Flatscher, A. Ringhofer, G. Schickhofer, and A. Thiel. “Cross Laminated Timber (CLT): overview and development.” In: European Journal of Wood and Wood Products 74 (2016), pp. 331–351.

[7] U. Mantau. Real potential for changes in growth and use of EU forests. Final report. Hamburg/Germany. 2010.

[8] L. Franzoni, A. Lebée, F. Lyon, and G. Foret. “Influence of orientation and number of layers on the elastic response and failure modes on CLT floors: modeling and parameter studies.” In: European Journal of Wood and Wood Products 74 (2016), pp. 671–684.

[9] G Silly, A Thiel, and M Augustin. “Options for the resource optimized production of Laminar load carrying members based on wood products”. In: 10th World Conference on Timber Engineering, WCTE 2016, pp. 1320–1322.

[10] L. Wang and H. Ge. “Hygrothermal performance of cross-laminated timber wall assemblies: A stochastic approach.” In: Building and Environment 97 (2016), pp.11-25.

[11] S. Kordziel, S.V. Glass, C.R. Boardman, R.A. Munson, S.L. Zelinka, S. Pei, and P.C. Tabares-Velasco. “Hygrothermal characterization and modeling of cross-laminated timber in the building envelope.” In: Building and Environment 177 (2020), 106866.

[12] EN 16351: Timber structures – Cross laminated timber – Requirements. Bruxelles, Belgium: European Committee for Standardization CEN, 2021.

[13] EN 408: Timber structures – Structural timber and glued laminated timber – Determination of some physical and mechanical properties + A1. Bruxelles, Belgium: European Committee for Standardization CEN, 2012.

[14] EN 338: Structural timber – Strength classes. Bruxelles, Belgium: European Committee for Standardization CEN, 2016.

[15] GOM: ARAMIS user manual, ARAMIS. Gesellschaft für optische Messtechnik (GOM), Braunschweig, Germany. 2018.

[16] Dassault Systèmes SIMULIA 2022. ABAQUS Analysis User’s Manual. http://www.3ds.com/.

[17] Stora Enso. https://www.storaenso.com/-/media/documents/download-center/documents/product-specifications/wood-products/clt-technical/clt-by-stora-enso-technical-documentation---building-physics--2021-9-en.pdf

[18] Fraunhofer IBP. https://wufi.de/

[19] EN ISO 6946: Building components and building elements – Thermal resistance and thermal transmittance – Calculation methods. Bruxelles, Belgium: European Committee for Standardization CEN, 2017.

[20] WoodSolutions. Mid-rise Timber Building Structural Engineering Appendix 2: Worked Example for a CLT Mass Timber Panel Apartment Building A2. 2019.

https://doi.org/10.52202/080513-0277